A nonlinear analysis of the transport Barkhausen-like noise measured in $(Bi,Pb)_2Sr_2Ca_2Cu_3O_{10+\delta}$ superconductors

I. García-Fornaris, H. Millán, R. F. Jardim, and E. Govea-Alcaide'

Citation: Chaos **23**, 023116 (2013); doi: 10.1063/1.4807682
View online: http://dx.doi.org/10.1063/1.4807682
View Table of Contents: http://aip.scitation.org/toc/cha/23/2
Published by the American Institute of Physics

A nonlinear analysis of the transport Barkhausen-like noise measured in $(Bi,Pb)_2Sr_2Ca_2Cu_3O_{10+\delta}$ superconductors

I. García-Fornaris,[1] H. Millán,[1] R. F. Jardim,[2] and E. Govea-Alcaide[1,a)]
[1]*Departamento de Ciencias Básicas, Facultad de Ciencias Técnicas, Universidad de Granma, Apdo. 21, P. O. Box 85100 Bayamo, Cuba*
[2]*Instituto de Física, Universidade de São Paulo, CP 66318, 05315-970 Sãod Paulo, SP, Brazil*

(Received 4 December 2012; accepted 1 May 2013; published online 23 May 2013)

We investigated the transport Barkhausen-like noise (TBN) by using nonlinear time series analysis. TBN signals were measured in $(Bi,Pb)_2Sr_2Ca_2Cu_3O_{10+\delta}$ ceramic samples subjected to different uniaxial compacting pressures (UCP). These samples display similar intragranular properties but different intergranular features. We found positive Lyapunov exponents in all samples, $\lambda_m \geq 0.062$, indicating the nonlinear dynamics of the experimental TBN signals. It was also observed higher values of the embedding dimension, $m > 9$, and the Kaplan-Yorke dimension, $D_{KY} > 2.9$. Between samples, the behavior of λ_m and D_{KY} with increasing excitation current is quite different. Such a behavior is explained in terms of changes in the microstructure associated with the UCP. In addition, determinism tests indicated that the TBN masked deterministic components, as inferred by $|\vec{k}|$ values larger than 0.70 in most of the cases. Evidence on the existence of empirical attractors by reconstructing the phase spaces has been also found. All obtained results are useful indicators of the interplay between the uniaxial compacting pressure, differences in the microstructure of the samples, and the TBN signal dynamics. © *2013 AIP Publishing LLC*.
[http://dx.doi.org/10.1063/1.4807682]

The most important microstructural units of polycrystalline materials are the grains and the grain boundaries. In general, the physical properties of the grains are depressed at the grain boundaries, resulting in different features of the specimen. In high-T_c superconductors, the transport critical current density decreases between three to five orders of magnitude with respect to the value measured within the grains of $\sim 10^8$ A/cm^2. Thus, several sintering techniques have developed to improve the transport critical current density across the grain boundaries in these materials. At the same time, other experimental techniques intend to study the influences of the synthesis on the microstructure and therefore on the superconducting critical current density. One of these techniques is the Transport Barkhausen-like Noise (TBN), which measures the voltage across the sample under the simultaneous influence of a DC excitation current and a low frequency AC applied magnetic field. In this work, we performed a nonlinear analysis of the TBN signals measured in high-T_c polycrystalline superconductors subjected to different uniaxial compacting pressure before the last heat treatment. The obtained results reveal that the TBN signal has a clear chaotic nature. Also, it was possible to establish a relationship between the behavior of some nonlinear parameters and the microstructure of the studied samples. The main conclusion of the work is that both the TBN signal and the nonlinear analysis are useful tools to study the influence of microstructure on the transport critical current density of polycrystalline samples of high-T_c superconductors.

I. INTRODUCTION

The granular nature of polycrystalline high-T_c superconductors is the most important limitation for the large scale applications of these materials.[1] In ceramic materials, it is possible to identify two important microstructural units: the grains and the grain boundaries (GB), also referred to as the intragranular and the intergranular regions, respectively. In the intergranular region, the presence of voids, cracks, impurities, oxygen non-stoichiometry, and the misorientation between adjacent grains are responsible for a decrease by three to five orders of magnitude in the transport critical current density, J_c. The impact of the above microstructural factors on the electromagnetic properties of these materials greatly depends on the sintering conditions. The use of different types of mechanical deformation is one of the most extended solution to improve J_c mainly due to its marked increase in the degree of texture of the samples, which tends to strengthen the connectivity between adjacent grains.[2]

In previous studies, we have described the influence of the uniaxial compacting pressure (UCP) on the general superconducting properties of $(Bi,Pb)_2Sr_2Ca_2Cu_3O_{10+\delta}$ (Bi-2223) ceramic samples.[3,4] The most important feature of these samples is that they exhibited similar intragranular properties but different intergranular ones. Moreover, the experimental results were consistent with the occurrence of three different superconducting levels in the samples: (i) the superconducting grains; (ii) the superconducting clusters; and (iii) the weak-links.[4,5] As the properties of the last two levels are very sensitive to the UCP, these samples constitute an excellent tool to testing novel techniques sensitive to processes occurring at the intergranular level.

a)Electronic mail: egoveaa@udg.co.cu.

Within this scenario, a novel technique referred to as Transport Barkhausen-like noise (TBN) was reported in the last decade.[6] The authors subjected a polycrystalline YBCO specimen to a low-frequency triangular-wave magnetic field, $B_a(t)$ along with a dc electrical current, and measured the voltage across the sample. Increasing $B_a(t)$ resulted in the penetration of the magnetic field within the sample. In such an experiment, when the maximum applied magnetic field, B_{max}, is less than the first thermodynamic critical field of grains, magnetic flux only penetrates the weak-links and/or the superconducting clusters.[4] In addition to this, the distribution of the intergranular magnetic field within the sample is determined by its intergranular features or more appropriately to its microstructure. The combination of the above physical ingredients resulted in a measurable voltage noise, stemming from the flux-creep to the flux-flow transition of Josephson vortex at the intergranular level.[7,8] The observed abrupt jumps in TBN signals were correlated to pinning and depinning of the Josephson vortices in a background comprised of random pinning centers. Such an irregular motion in turn is responsible for changes in the distribution of the intergranular applied magnetic field and thus of the electrical current throughout the sample. The simultaneous superconducting to normal-state transition of several weak-links (resistive transition) generates a series of avalanche in the electrical current rearrangement within the sample, generating a voltage noise that is measured.[9] These signals differ from the conventional magnetic Barkhausen noise (MBN), where fluctuations in the voltage signal correspond to sudden and discontinuous jumps in the magnetization of the material.[10] In TBN measurements, the discontinuous jumps are also predicted to occur but in the magnetoresistance data.[6]

The first TBN study in polycrystalline samples of $(Bi,Pb)_2Sr_2Ca_2Cu_3O_{10+\delta}$ (Bi-2223) was reported recently.[12] However, a systematic study of the effects of the excitation current on TBN signals measured in Bi-2223 samples subjected to different UCP was performed more recently.[11] The analysis of the experimental data confirmed that the power spectrum of the TBN follows a $1/f^n$ law with $n \sim 2$ and is independent of the excitation current.[6,12] Also, a simple correlation between the excitation current and the time or the applied magnetic field where the noise first appears (see Fig. 1) revealed differences in the granular structure of the samples, previously detected by other traditional techniques.[3,4]

Based on the nonlinear nature of the electrical-current characteristic of the grain boundaries, we have proposed a model for the TBN in high-T_c materials.[13] A series-parallel array of Josephson junctions was considered and details of the microstructural features of the samples were taken into account, as changes in the angle of adjacent grains. The model reproduced qualitatively well the changes in both the width and the intensity of the TBN. In spite of the above investigations point out for a possible nonlinear nature of the TBN signal, a systematic study on this matter is still lacking.

We thus report here a nonlinear analysis of the transport Barkhausen-like noise measured in $Bi_{1.65}Pb_{0.35}Sr_2Ca_2Cu_3O_{10+\delta}$ ceramic samples subjected to different uniaxial compacting pressures. The TBN signals were studied by using the TISEAN Software Package.[14] This package allows

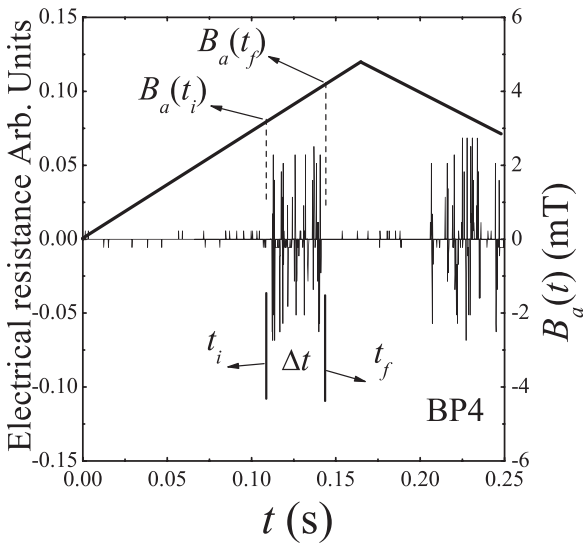

FIG. 1. Transport Barkhausen-like noise TBN measured in sample **BP4** for a normalized excitation current density $J_{ex}/J_c(0) = 0.5$, where $J_c(0)$ is the critical current density at zero applied magnetic field. The *ac* triangular applied magnetic field, $B_a(t)$, used in all measurements is also shown in the Figure. $\Delta t = t_i - t_f$ represents the time width in which the TBN signal occurs.

the nonlinear analysis directly from the scalar time series of the experimental data without an explicit construction of a mathematical model. While this computational effort has been successfully tested in physiological signals and climate data, to our knowledge, its performance was not explored within the context of the TBN signals. The aim of this study is to investigate the well known effect of the uniaxial compacting pressure on the microstructure of the samples but by extracting and inspecting the behavior of some nonlinear parameters such as the embedding dimension (m), the Kaplan-York dimension D_{KY}, and the maximal Lyapunov exponent (λ_m).

II. EXPERIMENTAL AND NONLINEAR ANALYSIS

Polycrystalline samples of $Bi_{1.65}Pb_{0.35}Sr_2Ca_2Cu_3O_{10+\delta}$ (Bi-2223) were prepared from powders of Bi_2O_3, PbO, $SrCO_3$, $CaCO_3$, and CuO, which were mixed in an atomic ratio of Bi:Pb:Sr:Ca:Cu (1.65:0.35:2:2:3). Details of the sample preparation are described elsewhere.[4] Before the last heat treatment, the powders were uniaxially pressed at different compacting pressures. The samples referred to as **BP2** and **BP4** were uniaxially pressed at 99 and 198 MPa, respectively (see Table I). The typical dimensions of the pellets were $d = 15$ mm in diameter and $h = 1$ mm in height. The last heat treatment was performed in air at 845 °C for 40 h followed by slow cooling.

We have evaluated the phase identification in both powder and bulk samples by means of X-ray diffraction patterns obtained in a Bruker-AXS D8 Advance diffractometer. These measurements were performed at room temperature using Cu Kα radiation in the $3^\circ \leq 2\theta \leq 80^\circ$ range with a 0.05° (2θ) step size and 5 s counting time. From the X-ray diffraction data, we evaluate the texture degree along the ($00\,l$) direction by calculating the Lotgering factor,

TABLE I. Some parameters of the samples studied in this work: the compacting pressure, P, the Lontgering factor along $(00\,l)$ direction, $F_{(00l)}$, the onset superconducting critical temperature, T_{on}, the offset superconducting critical temperature, T_{off}, the effective intergranular pinning energy, U_0, and the transport critical current density at zero applied magnetic field, $J_c(0)$, and 77 K. The parameters were extracted from Ref. 3.

Sample	P (MPa)	$F_{(00l)}$	T_{on} (K)	T_{off} (K)	U_0(1 mT) (eV)	$J_c(0)$ (A/cm^2)
BP2	99	0.54	119.5	98	2.1	142
BP4	198	0.70	120.2	105	7.5	461

$F_{(00l)} = (P - P_0)/(1 - P_0)$.[3] Here, $P_0 = I_{0(00l)}/\sum I_{0(hkl)}$ and $P = I_{(00l)}/\sum I_{(hkl)}$. Here, $I_{0(00l)}$ and $I_{0(hkl)}$ are the intensities of $(00\,l)$ and (hkl) peaks for a powder sample, respectively. On the other hand, $I_{(00l)}$ and $I_{(hkl)}$ are the intensities of $(00\,l)$ and (hkl) peaks, respectively, for the pellet sample.

Magnetization measurements under low applied magnetic fields were performed by using of a commercial Quantum Design SQUID magnetometer. In these experiments, the powder of a given sample was cooled in zero applied magnetic field from room temperature down to 77 K. After this, the applied magnetic field B_a was then increased from 0 to 50 mT, in steps of 0.5 mT and the magnetization was measured for each value of B_a.

Three types of transport measurements were performed by using the standard dc four-probe technique: (i) the temperature dependence of the electrical resistivity, $\rho(T)$, (ii) the current-voltage (I–V) characteristic curves, and (iii) the transport Barkhausen-like noise (TBN). In these measurements, copper electrical leads were attached to Au film contact pads of ~1400 Å in thickness, evaporated on parallelepiped-shaped samples using Ag epoxy. The typical dimensions of the samples were $t = 0.5$ mm (thickness), $w = 2$ mm (width), and $l = 10$ mm (length).

The temperature dependence of the electrical resistivity, $\rho(T)$ was measured in the temperature range $70\,\text{K} \leq T \leq 300\,\text{K}$. Before each measurement, the samples were cooled from room temperature down to 70 K. Then, an excitation current, $I = 1$ mA, was injected along the major length of the samples. The voltage across the sample and the temperature were both collected, while the temperature was raised slowly to 300 K.

Current-voltage I–V measurements were performed after cooling the sample in zero applied magnetic field to $T = 77$ K. Once the temperature was stabilized, the excitation current through the sample was applied and increased automatically in steps of 1 mA, while the voltage across the sample was measured. We extracted the value of the transport critical current at zero applied magnetic field, $I_c(0)$, from the measured I–V curve by taking the I_c value in which the voltage across the sample reaches 1 μV/cm.

The transport Barkhausen-like noise (TBN) was performed by using the standard dc four-probe technique. Details of the experimental setup are reported in the Ref. 11. In these experiments, the sample is always cooled from room temperature down to 77 K in zero applied magnetic field. After the cooling, a dc excitation current was applied to the sample along the plane perpendicular to the compacting direction. In order to assure that the signal only involves contributions arising from the magnetic field in the intergranular region, we have applied magnetic fields lower than the first thermodynamic critical field of the grains, H_{c1g}, which, in Bi-2223 samples, is believed to be ~ 8 mT at 77 K, as determined from the experimental $M(B_a)$ curves.[4]

III. THE NONLINEAR ANALYSIS

The nonlinear time series analysis was performed following the steps: (i) nonlinear noise reduction; (ii) minimal embedding delay determination after averaged mutual information estimation; (iii) embedding dimension determination after fraction of false nearest neighbors calculation; (iv) maximal Lyapunov exponent estimation; (v) phase space reconstruction; (vi) determinism tests; and (vii) determination of the Kaplan-Yorke dimension. Details of the procedure used in these steps are given below.

A. Nonlinear noise reduction

It is important to point out that each measurement process is inevitably sensitive to random or deterministic fluctuations. These undesired contributions can be minimized by using a locally projective nonlinear noise reduction filter. Here, we have used the filter developed in Ref. 15 The method is based on the hypothesis that a natural time series is a combination of both a low-dimensional dynamical system and a high-dimensional (random) noise. Unlike linear filters, the nonlinear ones are capable in removing only those noisy data points. The noise points are then replaced by estimates computed from a nonlinear interpolation process.[16,17] For this assignment, we have used the *ghkss.exe* program in the TISEAN Software Package.

B. Embedding delay determination

The mutual information (M_I) method was used for estimating an appropriate embedding delay value, τ.[18] The autocorrelation function for defining a convenient τ value has been used frequently. However, while the autocorrelation function describes only linear correlations, the mutual information also takes into account the nonlinear structures. That is, the mutual information between the TBN signals x_i and $x_{(i+\tau)}$ quantifies the information at a given state $x_{(i+\tau)}$ under the assumption that the information at the state x_i is known. The theoretical rationale of this method has been discussed elsewhere.[18,19] Here, we just describe its fundamental basis. Given a time series of TBN signals $x_0, x_1, x_2, \ldots, x_i, \ldots, x_k$ with minimum (x_{min}) and maximum (x_{max}) values, one is able to calculate the absolute difference $|x_{max} - x_{min}|$. This difference is partitioned into η equally sized intervals. Assuming j as large as a possible integer number, we would have

$$M_I = -\sum_{h=1}^{j}\sum_{\gamma=1}^{j} P_{h,\gamma}(\tau)\ln\frac{P_{h,\gamma}(\tau)}{P_h P_\gamma}, \tag{1}$$

where P_h and P_γ are the probabilities that the variable takes a value within the hth and γth levels, respectively, and $P_{h,\gamma}(\tau)$

is the joint probability in which x_i is in the h level and $x_{i+\tau}$ is in the γ level. The case $P_{h,\gamma}(\tau) = P_h P_\gamma$ implies no correlation between x_i and $x_{i+\tau}(M_I(\tau) \to 0)$. Generally, the first minimum of $M_I(\tau)$ versus τ is accepted as a suitable value for the time lag (τ). This allows us to derive the attractor reconstruction from the real time series. Also, it has been pointed out that the first minimum criterion only applies to a well marked minimum.[18] In the present work, this method was implemented by using the routine *mutual.exe* of the TISEAN Software Package. We allowed the search for the first minimum of $M_I(\tau)$ versus τ by setting $\tau_{max} = 500$ and $\eta = 12$ as starting parameters.

C. Embedding dimension

Kennel *et al.* suggested the fraction of false nearest neighbors (FFN) method for computing the minimal embedding dimension m.[14,19] This method allows one to reconstruct the phase space and unmask the deterministic structure of the system. Briefly, one constructs a vector sequence $\vec{p}(i) = x_i, x_{i+\tau}, x_{i+2\tau}, \ldots, x_{i+(m-1)\tau}$ (τ is the embedding delay) from each point in the m-dimensional embedding space. The next step is find a neighbor $\vec{p}(j)$, provided that $|p(i) - p(j)| < \varepsilon$, where ε is a small constant usually of the order of the standard deviation of the time series. Then, a normalized distance Γ_i between the $(m+1)$th embedding coordinate of points $p(i)$ and $p(j)$ could be computed

$$\Gamma(i) = \frac{|x_{i+m\tau} - x_{j+m\tau}|}{|p(i) - p(j)|}. \tag{2}$$

When the distance of the iteration to the nearest neighbor ratio exceeds a defined threshold (ε), the point is considered as a false neighbor. The outcome is a fraction (e.g., percentage) of false neighbors for each embedding dimension. For a correct application of this method, it is necessary to provide τ and ε values previously estimated. In addition to this, it is also required to introduce a range of m values, provided that FNN $\to 0$ with a significant number of points entering the statistics for the selected m range. In the present work, we set $m_{min} = 1$ to $m_{max} = 15$ as input parameters. The routine *false_nearest.exe* of the TISEAN Software Package was used as a computational tool.

D. Maximal Lyapunov exponent

The maximal Lyapunov exponent is the most common indicator of chaotic behavior of a system. This parameter characterizes the separation rate of trajectories within the phase space.[20] We have used the method developed in Ref. 21. In such a method, one considers the time series as a sequence $x_0, x_1, x_2, \ldots, x_i, \ldots, x_k$, where x_i represents the observation at time $i = 0, 1, 2, \ldots, N$. The data are treated as a trajectory and it is introduced the Euclidean distance $Y = |x_n - x_{n'}|$, representing a small perturbation. The evolution of Y is then estimated from the time series as

$$S(\varepsilon, m, \Delta t) = \log \sum |x_{n+t} - x_{n'+t}| = b + \lambda_m \Delta t, \tag{3}$$

where ε is the spacing within a two dimensional level constructed for defining nearest neighbors, Δt is the time interval, λ_m is the maximum Lyapunov exponent, and b is the intercept of the regression line. The slope of regressing $S(\varepsilon, m, \Delta t)$ on Δt is the estimate of the maximal Lyapunov exponent (λ_m). The $S(\varepsilon, m, \Delta t)$ versus Δt linear relationship needs to be confirmed for a range of grid spacing, ε. Here, we have selected five different ε values according to the ratio $\varepsilon_{max}/\varepsilon_{min} = 10$. A complete description of the method is found in Ref. 21. Based on λ_m values, three cases are distinguished from physical systems:

(a) $\lambda_m < 0$, representing a dissipative dynamical system with asymptotic stability;
(b) $\lambda_m = 0$, characterizing conservative dynamical systems. This is expected to be a very rare case for open, real systems like soils;
(c) $\lambda_m > 0$, related to the exponent of unstable and chaotic systems. This situation is not incompatible with the existence of some type of organization and/or pattern emergence (e.g., fractal or multifractal structures).

The program *lyap_k.exe* of the TISEAN project was selected for numerical computations.

E. Phase space reconstruction

The Takens theorem, delay method,[22] has been extensively used for the phase space reconstruction.[23,24] This theorem is applicable to infinitely long time series. The method may be used for embedding a univariate empirical time series x_i (i = 1, 2, …, N) into an m-dimensional space[23]

$$X_i^m = (x_i, x_{i+\tau}, \ldots, x_{i+(m-1)\tau}). \tag{4}$$

This method reconstructs the orbit

$$X_i^m = [x_1, x_2, \ldots, x_p]^\tau \quad p = N - (m-1), \tag{5}$$

where m is the embedding dimension and τ is the embedding delay. The routine *delay.exe* of the TISEAN package is appropriate for generating the time delay coordinates and to reconstruct the phase space.

F. Determinism tests

To investigate if the apparently randomness of the TBN signal has a hidden deterministic component, we perform a numerical test developed by Kaplan and Glass.[25] The embedding space is partitioned into L identical boxes. This method associates a unit vector field ($\hat{e}$) to the bundle of trajectories and searches for the directional variation of the vector field in its path through the L-th box. The directional behavior of the vector field determines three situations on the average length of the unit vectors associated to each trajectory (let us call $\vec{k}$):

(a) $\vec{k} \approx 1$, where the vectors crossing the L-th box are parallel to each other. In this case the system might be defined as highly deterministic.
(b) $\vec{k} \approx 0$, where all the vectors crossing the L-th box are randomly oriented each other. In this case, the trajectories intercept each other at any angle, reducing the

average vector length. This occurs for stochastic (random) systems.

(c) $0 \leq \vec{k} \leq 1$, where the system masks both determinist and stochastic components. The predominant component here is determined by the $\vec{k}$ value.

In this case, the program *determinism.exe* was used for numerical computations[26] and applied to both filtered and non-filtered TBN signals. One of the final results constitutes the average $|\vec{k}|$ value. In our calculations, the number of boxes is L = 30.

G. The Kaplan-Yorke dimension

The Kaplan-Yorke dimension (D_{KY}) is an interesting nonlinear parameter as it is usually related to the complex structure of the attractor, confining the dynamics of the system. It was originally stated as a conjecture,[27] but it has proved to be true. Many authors consider D_{KY} as a measure of complexity, strangeness, and fractal dimension of the attractor.[14,28] In addition, D_{KY} also has been identified as the dimension of the system.[29] The practical computation of D_{KY} requires the spectrum of Lyapunov exponents. By considering a chaotic system with m degree of freedom (m embedding dimensions or delay coordinates), the Lyapunov exponents spectrum is expected to have as many exponents as degree of freedom. Let us consider a N-dimensional system such that its spectrum of Lyapunov exponents contains n exponents. If $\sum$ is the sum from λ_1 to λ_n, such that $n \leq N$, then there exists a maximum integer number $n = \omega$ such that $\sum$ is still positive and another integer $\omega + 1$ such that $\sum$ is negative. It is then hypothesized that the fractal dimension of the studied system locates between ω and $\omega + 1$. The mathematical expression for such a computation is

$$D_{KY} = n + \frac{\sum_{i=1}^{n} \lambda_i}{|\lambda_{n+1}|}, \tag{6}$$

where n is the maximum integer such that the sum of the n largest Lyapunov exponents is still positive.

It is instructive to illustrate here the application of Eq. (6) for the case of the well known Lorenz system. The Lyapunov exponent spectrum for such a system is composed by $\lambda_1 = 0.90564, \lambda_2 = 0.0,$ and $\lambda_3 = -14.57231$ (an extremely large negative exponent). The application of Eq. (6) yields $\lambda_1 + \lambda_2(n = 2) = 0.90564$ and $|\lambda_{n+1}| = 14.57231$. Thus, $D_{KY} = 2 + (0.90564/14.57231) = 2.06214$, suggesting that the negative Lyapunov exponent adds a strong deterministic component to the system dynamics. In fact, the determinism test as applied to the Lorenz system renders $|\vec{k}| = 0.998$.

From nonlinear time series analysis, one may define the Lyapunov time, Λ, as

$$\Lambda = \frac{T}{\lambda_m}, \tag{7}$$

where T is the experimental sampling interval. The Λ parameter represents the maximal time period for making reliable predictions. Equation (7) has been used previously within a climatic perspective.[30]

IV. RESULTS AND DISCUSSION

Some preliminary features of the studied samples are of interest and can be find elsewhere.[3,11,31] We first mention that X-ray diffraction patterns revealed that all samples have similar chemical composition and their indexed reflections are related to the high-T_c Bi-2223 phase.[3] Values of the Lotgering factor reported in Table I were found to increase ~30% between sample **BP2** ($F_{(00l)} = 0.54$) and sample **BP5** ($F_{(00l)} = 0.70$). This result indicates that both samples have different degree of texture and that grains of the sample **BP4** are more aligned than those of sample **BP2**. Such a feature has its counterpart in the intergranular transport properties of the samples. From curves of the temperature dependence of the electrical resistivity, $\rho(T)$, we have found that the superconducting transition temperature of isolated grains T_{on} is essentially the same for both samples but T_{off}, the temperature in which the zero-resistance state is observed, increases from 98 (sample **BP2**) to 105 K (sample **BP4**), as displayed in Table I. This corroborates the assumption that both samples have similar intergranular properties but quite different intergranular ones.

We also mention that increasing the uniaxial compacting pressure improves the texture degree which and the connectivity between grains. As a consequence, the transport critical current density, which strongly depends of the features at the intergranular level, increases ~3 times (see Table I). Similar improvement has been also observed in the behavior of the intergranular pinning energy. In this case, increasing compacting pressure results in the dynamics of the Josephson vortices, mostly those located at the grain boundaries. In summary, the intergranular features of samples **BP2** and **BP4** are different and may be used for testing the transport Barkhausen-like noise technique as a tool for a better understanding of superconducting ceramic samples, as discussed elsewhere.[6]

Measurements of the transport Barkhausen-like noise were then performed in order to gain further information regarding the intergranular properties of the samples. Figure 1 displays the time dependence of the TBN signal, in which the measured voltage across the sample is transformed into electrical resistance (sample **BP4**) for a given fraction of the normalized excitation current density, $J_{ex}/J_c(0) = 0.5$. Here, J_{ex} is the excitation current applied to the sample. We have also included in the figure the *ac* waveform of the applied magnetic field, $B_a(t)$. The maximum value of $B_a(t)$ used in all measurements was 5.5 mT. The noise appears in a time interval $\Delta t = t_f - t_i$, where t_i is the time in which the noise signal first appears and t_f is the time where it vanishes. The occurrence of the TBN signal has been detected in a narrow region of $B_a(t)$ or more appropriately between the corresponding magnetic fields $B_a(t_i)$ and $B_a(t_f)$, as inferred from the Figure 1. The TBN signals measured in samples **BP2** and **BP4**, subjected to different values of the normalized excitation current density, $J_{ex}/J_c(0)$, revealed an appreciable decrease of t_i with increasing excitation current.[11] We also

mention that such a behavior is much more pronounced in sample **BP2**. Similar behavior has been observed in both t_f and $B_a(t_f)$. Also, the intensity of the TBN signal is much higher in sample **BP2**. As pointed out above, there is a definite microstructural difference between the uniaxially pressed samples. As the detected TBN signal stems from pinning and depinning processes at the intergranular medium, the general physical behavior of the samples may be related to the differences in their intergranular features.

We turn now to the nonlinear analysis of the TBN signals for different values of the ratio $J_{ext}/J_c(0)$ (see Fig. 4 of Ref. 11). We emphasize that our samples have three different initial parameters: (i) the ratio $J_{ext}/J_c(0)$; (ii) the *ac* triangular applied magnetic field, $B_a(t)$; and (iii) the microstructure which is uniaxial compacting pressure dependent. The relevant results for the analysis are displayed in Table II and may be summarized as follows: (i) all values of the maximal Lyapunov exponent are positive, strongly suggesting the existence of chaotic behavior in the TBN signals; (ii) the occurrence of high values of the embedding dimension, m, and the Kaplan-Yorke dimension, $D_{KY;}$ (iii) a reduction of the embedding dimension between samples **BP2** and **BP4**. As m is related to the active number of degrees of freedom, its high values indicate that many variables have an effect on the nonlinear evolution of the TBN signal. We also notice that in the sample **BP4** and for any $J_{ext}/J_c(0)$ ratio, values of m are smaller than those obtained for the sample **BP2**. According to the meaning of the maximal Lyapunov exponent, the results displayed in Table II indicate that sample **BP2** is much less sensitive to changes in the initial conditions ($J_{ext}/J_c(0)$) than **BP4**. Consequently, as the ratio $J_{ext}/J_c(0)$ increases, the dynamics of the TBN signal measured in the sample **BP2** remains essentially unaltered while it varies appreciably in sample **BP4**. It is important to notice that, given the three initial conditions, two of them, $J_{ext}/J_c(0)$ and $B_a(t)$ are similar in both samples. On the other hand, their microstructures are quite different by the virtue of the unixial compacting pressure. Thus, it is reasonable to connect the changes observed in the nonlinear parameters displayed in Table II to the microstructural differences between samples.

Let us then consider that the polycrystalline samples studied here are comprised of three superconducting levels: the superconducting grains, the superconducting clusters, and the weak-links.[3,4] Within this scenario, the magnetic flux first penetrates the sample via the weak-links, a phenomenon believed to occur at very low applied magnetic $B \ll B_a(t)$ fields. With increasing $B_a(t)$, the magnetic flux starts to penetrate the superconducting clusters. A further increase in B_a, being higher than the first thermodynamic critical field, would result in a penetration of the magnetic flux within the superconducting grains. The sample **BP2** is believed to be comprised of superconducting grains which are weak coupled to each other. In other words, its pinning energy is quite low (see Table I) so intergranular vortices can move almost freely throughout the intergranular medium of the material. On the other hand, sample **BP4**, subjected to a much higher compacting pressure, is comprised of a microstructure of strong-coupled and well-connected superconducting grains, or more appropriately speaking, a microstructure composed mostly of superconducting clusters.

TABLE II. Nonlinear parameters of the TBN signals measured in the studied samples for different values of $J_{ext}/J_c(0)$: embedding dimension m, maximal Lyapunov exponent λ_m, and the Kaplan-Yorke dimension D_{KY}.

	BP2			BP4		
$J_{ext}/J_c(0)$	m	λ_m	D_{KY}	m	λ_m	D_{KY}
0.4	13	0.105	4.356	9	0.108	2.974
0.5	15	0.118	4.702	10	0.062	3.283
0.6	13	0.126	4.746	10	0.171	4.091
0.7	15	0.123	4.778	13	0.158	5.019
0.8	15	0.103	4.579	11	0.183	5.071

We now turn to the connection of the parameters extracted from the nonlinear analysis with the microstructure of the samples. Due to the difference in their microstructures, it is reasonable to assume that small changes in the nonlinear parameters, extracted from sample **BP2**, are related to two features: (i) its very low pining energy; and (ii) the very high population of high-angle Josephson junctions between adjacent grains, that act as weak-links. On the other hand, the high sensibility of λ_m to the increasing of the ratio $J_{ext}/J_c(0)$ in sample **BP4** is certainly due to the very high population of low-angle Josephson junctions, making the TBN signals being dominate by the superconducting clusters, as reported elsewhere.[11] These results also suggest, to some extent, that the uniaxial compacting pressure has its counterpart in the nature of the TBN signals and dynamics.

Some previous investigations on chaotic dynamics have suggested that noise is not responsible for inducing chaos,[32] while others have reported the occurrence of deterministic chaos in systems with $\lambda_m > 0$.[33,34] In the latter, chaos has been found within an experimental resonance circuit with nonlinear capacitors. The authors explained such a chaotic behavior in terms of an underlying collective cooperation of multiple domains where all degrees of freedom inside the ferroelectric capacitor cooperate. Following the above-mentioned statement, we consider that the chaotic behavior detected in the TBN signals may not be caused by a noisy signal component. In our view, the chaotic behavior deserves a more detailed description. We first recall that increasing the ratio $J_{ext}/J_c(0)$ implies in a superconductor to normal transition, a feature close connected to the population of grain boundaries with high angles.[35] That is, when a current channel, or pathway, through a weak-link is suppressed, the current density in the neighboring area is expected to increase and will continue to disrupt others weak-links. This results in a redistribution of the transport current throughout the sample, causing a nonlinear behavior due to the random movement of the vortices, expected to be pinned and depinned at the grains boundaries.

Values of D_{KY} are commonly associated with the attractor dimension or the information entropy of the system,[28] as well as the high dimensional structure of the system. In the latter case, higher values of D_{KY} are related to the existence of extreme Lyapunov exponents. This indicates a highly chaotic degree of freedom coming along with a dissipative

degree of freedom. This higher dimensionality may be detected from the embedding dimension m values. The D_{KY} values in the sample **BP2** remains almost unaltered as the ratio $J_{ext}/J_c(0)$ increases. In contrast, in sample **BP4**, D_{KY} values follow a linear trend. This constitutes an interesting result and may be related to the microstructural differences between samples. Notice that in sample **BP2**, the microstructure can be seen as more *isotropic* due to the high concentration of high angles between adjacent grains.[3,11,13] We want to remark that the occurrence of noise is due to pinning and depinning of Josephson vortices. Most of the junctions in this sample behave as weak-links, the orientational degree is low, and the pinning energy of the vortices is also very low (see the Table I). The combination of the above factors strongly indicates that this sample is almost insensitive to changes in the excitation current, or more appropriately to the ratio $J_{ext}/J_c(0)$. Let us again suppose that grain boundaries or junctions are the source of information in this set of samples. If an individual grain boundary or junction is in the superconducting state, we define its *informational state* as 0: in the normal-state it is 1. The results strongly suggest that the microstructure of the sample **BP2** is comprised of junctions with state 1 at the same time for a given excitation current, even for low values of $J_{ext}/J_c(0)$. Similar considerations were taken into account in the Ref. 35. The above analysis implies that the number of informational sources may not vary with increasing the excitation current. In the sample **BP4**, the analysis is somewhat different. This sample, pelletized in a higher uniaxial compacting pressure, is comprised of weak-links and some superconducting cluster, i.e., grains more strongly connected.[3,4,11] In this sample as the excitation current increases the number of informational sources also increase. For low excitation current, the weak-links have state 1 but cluster remains in 0. As the ratio $J_{ext}/J_c(0)$ increases some clusters change its state to 1, in consequence D_{KY} also increases. Within the framework of the above analysis, the conclusion stated that increasing the ratio $J_{ext}/J_c(0)$ contributes to the chaotic behavior of the samples. This is also supported by previous computational investigations in Josephson junctions systems.[36]

Returning to the data displayed in Table II, one also observes that sample **BP4** has larger λ_m values. Furthermore, we found a significant linear relationship between D_{KY} values and $J_{ext}/J_c(0)$ (the correlation coefficient is $R=0.972$). This indicates that dynamics of the TBN signal increases its complexity as a function of $J_{ext}/J_c(0)$. Thus, the fractal dimension of the attractor also increases. This experimental finding supports, to some extent, our hypothesis on the relationship between the fractal dimensionality of the attractor and the pinning energy. However, as compared with **BP2**, the dynamics of the TBN signal in the sample **BP4** seems to be influenced by a higher negative Lyapunov exponent for $J_{ext}/J_c(0)=0.4$, 0.5, and 0.6. Notice, that for these values of the excitation current D_{KY} (**BP4**) $< D_{KY}$ (**BP2**). It seems that for high $J_{ext}/J_c(0)$ values more stable oscillation modes dominate the TBN dynamics of the sample **BP4**. On the other hand, it is important to point out that the condition $m > 2D_{KY}$ has been fulfilled in all calculations, as usually considered within the context of nonlinear dynamics.[37]

The determinism test also rendered valuable results for a more detailed discussion.[25] For all considered cases, this parameter indicate the existence of a hidden determinist component driving the TBN dynamics. This expected result has been confirmed after conducting the same determinism test on the unfiltered TBN signals (see Table III). That is, all the apparently noisy signals mask a strong deterministic component ranging from $|\vec{k}|=74\%$ to $|\vec{k}|=90\%$ for the filtered signal and from $|\vec{k}|=51\%$ to $|\vec{k}|=71\%$ for the filtered and unfiltered signals, respectively. Thus, the chaotic dynamics is deterministic to some extent. These results could contradict, in principle, traditional findings derived from linear spectral analysis, which are used for detecting Gaussian noise. That is, the Fourier analysis represents a collection of linear methods which are insensitive to nonlinear response of the system. The determinist chaos suggests an underlying nonlinear deterministic structure that, in spite of the presence of noise, allows one to infer how much the deterministic structure is still visible and how much of this underlying structure is stochastic. These findings also suggest the existence of some sort of predictability range, as represented by the Lyapunov time Λ. Within the range of variables described above, deterministic models (e.g., local or global polynomial models) may be appropriate for describing the TBN signals. We also mention that, in Ref. 33, the authors have derived an ordinary differential equations ODE system for describing the nonlinear dynamics of a ferroelectric capacitor from experimental data analysis only.

Figure 2 shows the 2-dimensional phase space portrait projection, also referred as attractors, for the filtered TBN time series from the studied samples at $J_{ext}/J_c(0)=0.4$. Some components of the waveform were not successfully resolved but the presence of closed orbits is still visible. The dynamics is more dense for smaller oscillations (i.e., near the center of the orbit) where noise persists. Each inset represents the 2-D projection of this noise embedded in the m-dimensional space. The random distribution of points within a smaller spatial region is observed. This smaller area is concentrated around the state space center. These random points fill the space without any coherence or a clear structure. However, Fig. 2(b) displays a much better waveform resolution for the sample **BP4** when compared with that corresponding to sample **BP2**. A careful inspection of the attractor of the Fig. 2 strengthens the idea that the TBN signal is not only a noisy signal, in the sense that the respective behaviors of these signals are completely different from a

TABLE III. Results of the determinist test, $|\vec{k}|$, for the filtered and unfiltered TBN signals measured in the studied samples for different values of the ratio $J_{ext}/J_c(0)$.

	Filtered		Unfiltered	
$J_{ext}/J_c(0)$	BP2	BP4	BP2	BP4
0.4	0.81	0.85	0.67	0.64
0.5	0.79	0.65	0.66	0.60
0.6	0.80	0.74	0.57	0.69
0.7	0.75	0.90	0.51	0.71
0.8	0.79	0.77	0.69	0.68

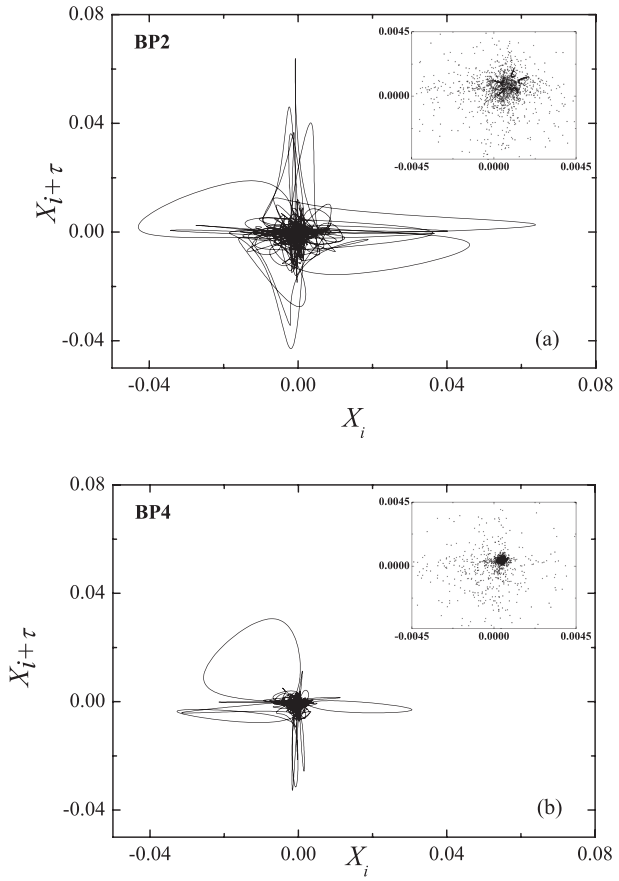

FIG. 2. 2-D phase space for the m-dimensional reconstructed orbit with time delayed coordinates of the filtered TBN series for $\tau = 4$ of (a) sample **BP2** and (b) sample **BP4**. The ratio $J_{ext}/J_c(0) = 0.4$ has been used for both samples. The inset displays the noisy component near the center of the orbit (see comments in the text).

colored noise. Moreover, the data displayed in Fig. 2 reveal the effect of the compacting pressure on the TBN behavior. Such an effect is mainly reflected on the magnitude of the noisy component of the TBN signal. This is shown in the insets of the figure, where a clear noise reduction is observed as the compacting pressure increases. Such a result, combined with determinism tests, is believed to be an useful indicator of the interplay between the uniaxial compacting pressure, differences in the microstructure of the samples, and the TBN dynamics. Studies are underway to clarify the potential advantages of the nonlinear analysis of TBN signals compared to others in the literature.[38]

V. CONCLUSIONS

We have considered nonlinear time series analysis for interpreting the transport Barkhausen-like noise in uniaxially pressed $(Bi,Pb)_2Sr_2Ca_2Cu_3O_{10+\delta}$ ceramic samples. The obtained results indicate that all values of the maximal Lyapunov exponent are positive, the occurrence of high values of the embedding dimension, and the Kaplan-Yorke dimension. The combined results are sufficient to support the conclusion that the TBN signals measured in both samples present a chaotic nature. The observed behavior of the nonlinear parameters between samples **BP2** and **BP4** is of interest. We first mention the mean value of the embedding dimension that decreases from ~14 to ~10. The analysis also indicates a close relation between the microstructure of the samples and the chaotic nature of the TBN. In this sense, the results suggest that the noise measured in the sample **BP2** is more insensitive to changes in the applied magnetic field and the excitation current. This has been related to the very low pinning energy at the intergranular medium, which is large comprised of weak-links. The excitation current affected significantly neither λ_m nor D_{KY} for **BP2** sample (it was not found a significant statistical relationship between D_{KY} and $J_{ext}/J_c(0)$) which provides no information on **BP2** sample microstructure. On the other hand, D_{KY} value increased following a linear relationship as a function of $J_{ext}/J_c(0)$ for **BP4** sample. Finally, our findings suggest that D_{KY} might better discriminator of the TBN dynamics than λ_m due to the underlaying influence of negative Lyapunov exponent on D_{KY} computations. This was more evident for **BP4** sample.

ACKNOWLEDGMENTS

This work was supported by the Brazil agencies FAPESP, CNPq, and CAPES. R.F.J. is CNPq fellow under Grant No. 304112/2010-0. The authors are indebted to L. R. Padovese and M. Alberteris-Campos for the laboratory facilities in the TBN measurements and E. Altshuler for the critical reading of the manuscript.

[1]D. Larbalestier, A. Gurevich, D. M. Feldmann, and A. Polyanskii, Nature **414**, 368 (2001).
[2]T. T. Tan, S. Li, H. Cooper, W. Gao, H. K. Liu, and S. X. Dou, Supercond. Sci. Technol. **14**, 471 (2001).
[3]E. Govea-Alcaide, I. García-Fornaris, P. Muné, and R. F. Jardim, Eur. Phys. J. B. **58**, 373 (2007).
[4]E. Govea-Alcaide, R. F. Jardim, and P. Muné, Physica C **423**, 152 (2005).
[5]L. Ji, M. S. Rzchowski, N. Anand, and M. Tinkham, Phys. Rev. B **47**, 470 (1993).
[6]P. Mazzetti, A. Stepanescu, and P. Tura, Phys. Rev. B **65**, 132512 (2002).
[7]A. Gurevich, Phys. Rev. B **46**, R3187 (1992).
[8]S. Ooi, T. Mochiku, and K. Hirata, Phys. Rev. Lett. **89**, 247002 (2004).
[9]L. Ponta, A. Carbone, M. Gilli, and P. Mazzetti, Phys. Rev. B **79**, 134513 (2009).
[10]V. Moorthy, B. A. Shaw, and S. Day, Acta Mater. **52**, 1927 (2004).
[11]I. García-Fornaris, E. Govea-Alcaide, M. Alberteris-Campos, P. Muné, and R. F. Jardim, Physica C **470**, 611 (2010).
[12]E. Govea-Alcaide, J. Anglada-Rivera, R. F. Jardim, and P. Muné, J. Magn. Magn. Mater. **299**, 231 (2006).
[13]I. García-Fornaris, P. Muné, P. A. Suzuki, M. Alberteris-Campos, R. F. Jardim, and E. Govea-Alcaide, Physica C **470**, 269 (2010).
[14]R. Hegger, H. Kantz, and T. Schreiber, Chaos **9**, 413 (1999).
[15]E. Ott, T. Sauer, and J. A. Yorke, *Coping with Chaos* (Wiley, New York, 1994).
[16]A. H. Jazwinski, *Stochastic Processes and Filtering Theory* (Academic Press, New York, 1970).
[17]A. C. Harvey, *Forecasting, Structural Time Series Models and the Kalman Filter* (Cambridge University Press, Cambridge, 1989).
[18]A. M. Fraser and H. L. Swinney, Phys. Rev. A **33**, 1134 (1986).
[19]M. B. Kennel, R. Brown, and H. D. I. Abarbanel, Phys. Rev. A **45**, 3403 (1993).
[20]J. C. Sprott, *Chaos and Time Series Analysis* (Oxford University Press, Oxford, 2003).
[21]H. Kantz, Phys. Lett. A **185**, 77 (1994).
[22]F. Takens, *Detecting Strange Attractors in Turbulence: Lecture Notes in Mathematics* (Springer, New York, 1981), Vol. 898.
[23]B. B. Li and Z. F. Yuan, J. Eng. Med. **222**, 265 (2008).

[24]H. Millán, B. Ghanbarian-Alavijeh, and I. García-Fornaris, Atmos. Res. **98**, 89 (2010).
[25]D. T. Kaplan and L. Glass, Phys. Rev. Lett. **68**, 427 (1992).
[26]M. Perc, see http://fizika.uni-mb.si/matjaz/ejp/time.html for user friendly programs for nonlinear time series analysis, version 5 (2004).
[27]J. Kaplan and J. Yorke, *Functional Differential Equations and Approximation of Fixed Points* (Springer, New York, 1987).
[28]J. C. Sprott, Chaos **17**, 33124 (2007).
[29]P. Frederickson, J. L. Kaplan, E. D. Yorke, and J. A. Yorke, J. Differ. Equations **49**, 185 (1983).
[30]S. Chaudhuri, Adv. Complex Syst. **9**, 77 (2006).
[31]I. García-Fornaris, A. A. Planas, P. Muné, R. F. Jardim, and E. Govea-Alcaide, J. Supercond. Novel Magn. **23**, 1511 (2010).
[32]B. Dennis, R. A. Desharnais, J. M. Cushing, S. M. Henson, and R. F. Costantino, Oikos **102**, 329 (2003).
[33]R. Hegger, H. Kantz, F. Schmüser, M. Diestelhorst, R. Kapsch, and H. Beige, Chaos **8**, 727 (1998).
[34]R. Kapsch, H. Kantz, R. Hegger, and M. Diestelhorst, Int. J. Bifurcation Chaos **11**, 1019 (2001).
[35]B. Zeimetz, B. A. Glowacki, and J. E. Evetts, Eur. Phys. J. B. **29**, 359 (2002).
[36]X. Huifen, F. Minhua, S. Yang, and W. Peiheng, J. Appl. Phys. **78**, 6664 (1995).
[37]H. Kantz and T. Schreiber, *Nonlinear Time Series Analysis* (Cambridge University Press, Cambridge, 2004).
[38]Y. Tsuchida, T. Ando, and M. Enokizono, IEEE Trans. Magn. **38**, 3210 (2002).